Restoring mitochondrial calcium uniporter expression in diabetic mouse heart improves mitochondrial calcium handling and cardiac function

Received for publication, January 23, 2018, and in revised form, March 26, 2018 Published, Papers in Press, April 6, 2018, DOI 10.1074/jbc.RA118.002066

Jorge Suarez[‡1], Federico Cividini[‡1], Brian T. Scott[‡], Kim Lehmann[§], Julieta Diaz-Juarez[‡¶], Tanja Diemer[‡], Anzhi Dai[‡], Jorge A. Suarez[‡], Mohit Jain[§], and Wolfgang H. Dillmann[‡2]

From the [‡]Department of Medicine, University of California, San Diego, La Jolla, California 92093-0671, the [§]Departments of Medicine and Pharmacology, University of California, San Diego School of Medicine, La Jolla, California 92093, and the [¶]Department of Pharmacology, Instituto Nacional de Cardiología, Juan Badiano 41, Barrio Belisario Domínguez Secc XVI, 14080 Tlalpan, DF, Mexico

Edited by Qi-Qun Tang

Diabetes mellitus is a growing health care problem, resulting in significant cardiovascular morbidity and mortality. Diabetes also increases the risk for heart failure (HF) and decreased cardiac myocyte function, which are linked to changes in cardiac mitochondrial energy metabolism. The free mitochondrial calcium level ($[Ca^{2+}]_m$) is fundamental in activating the mitochondrial respiratory chain complexes and ATP production and is also known to regulate pyruvate dehydrogenase complex (PDC) activity. The mitochondrial calcium uniporter (MCU) complex (MCUC) plays a major role in mediating mitochondrial Ca^{2+} import, and its expression and function therefore have a marked impact on cardiac myocyte metabolism and function. Here, we investigated MCU's role in mitochondrial Ca^{2+} handling, mitochondrial function, glucose oxidation, and cardiac function in the heart of diabetic mice. We found that diabetic mouse hearts exhibit altered expression of MCU and MCUC members and a resulting decrease in $[Ca^{2+}]_m$, mitochondrial Ca^{2+} uptake, mitochondrial energetic function, and cardiac function. Adeno-associated virus-based normalization of MCU levels in these hearts restored mitochondrial Ca^{2+} handling, reduced PDC phosphorylation levels, and increased PDC activity. These changes were associated with cardiac metabolic reprogramming toward normal physiological glucose oxidation. This reprogramming likely contributed to the restoration of both cardiac myocyte and heart function to nondiabetic levels without any observed detrimental effects. These findings support the hypothesis that abnormal mitochondrial Ca^{2+} handling and its negative consequences can be ameliorated in diabetes by restoring MCU levels via adeno-associated virus–based MCU transgene expression.

This work was supported by National Institutes of Health Grant HL066941, Merit Review Award BX001121 from the Department of Veterans Affairs, the P. Robert Majumder Charitable Foundation, University of California Institute for Mexico and the United States (UC MEXUS)-Consejo Nacional de Ciencia y Tecnología (CONACYT) Grant CN 15-1489 (to W. H. D. and J. D. J.). The authors declare that they have no conflicts of interest with the contents of this article. The content is solely the responsibility of the authors and does not necessarily represent the official views of the National Institutes of Health.

[1] Both authors contributed equally to the results of this work.

[2] To whom correspondence should be addressed: 9500 Gilman Dr., La Jolla, CA 92093-0671. Tel.: 858-534-9934; Fax: 858-534-9932; E-mail: wdillmann@ucsd.edu.

Diabetes-related cardiac dysfunction is caused by multiple factors. Mitochondrial dysfunction has been proposed as a principal pathophysiological mechanism in the development of diabetic heart disease (1). Abnormal mitochondrial Ca^{2+} handling has been identified as contributing to mitochondrial dysfunction, although the mechanisms causing this alteration are not well understood (1). Numerous studies have shown that mitochondrial Ca^{2+} uptake is decreased in cardiac myocytes (CM)[3] from the diabetic heart (2–4), yet the degree to which the decreased CM free mitochondrial Ca^{2+} concentration ($[Ca^{2+}]_m$) modulates decreased mitochondrial and cardiac function is currently unclear.

$[Ca^{2+}]_m$ is an important signaling mechanism for mitochondrial energetic activity. $[Ca^{2+}]_m$ enhances the activity of oxidative phosphorylation, especially mitochondrial complexes I, III, IV, and the V_{max} of complex V, leading to enhanced ATP formation (5). In addition, several dehydrogenases in the mitochondrial matrix (MM) are activated by $[Ca^{2+}]_m$ including the pyruvate dehydrogenase complex (PDC), which is key to glucose oxidation. $[Ca^{2+}]_m$ can either directly exert allosteric activation of PDC or increase PDC kinetics, reducing PDC phosphorylation via activation of mitochondrial PDC phosphatases (PDPs) (6, 7).

The heart is able to metabolize exogenous substrates such as glucose and free fatty acids (FA) to produce ATP, although FA are preferred (60–70%) (8, 9). However, the diabetic heart is energetically almost completely dependent on mitochondrial FA oxidation as a consequence of elevated levels of circulating FA and decreased intracellular glucose availability (10, 11). Maintaining dynamic glucose utilization in the presence of FA is essential for optimal cardiac function for the following reasons. 1) ATP produced from glycolysis could be preferentially used by the sarcoplasmic reticulum (SR) to fuel Ca^{2+} uptake

[3] The abbreviations used are: CM, cardiac myocytes; $[Ca^{2+}]_m$, mitochondrial Ca^{2+} concentration; MM, mitochondrial matrix; PDC, pyruvate dehydrogenase complex; FA, fatty acid; SR, sarcoplasmic reticulum; MCU, mitochondrial Ca^{2+} uniporter; MCUC, MCU complex; STZ, streptozotocin; qPCR, quantitative PCR; AAV, adeno-associated virus; IM, intramuscular injection; RCR, respiratory control ratio; BisTris, 2-[bis(2-hydroxyethyl)amino]-2-(hydroxymethyl)propane-1,3-diol; FCCP, carbonyl cyanide *p*-trifluoromethoxyphenylhydrazone; 2DG, 2-deoxy-D-glucose; ANOVA, analysis of variance; $[Ca^{2+}]_i$, cytosolic Ca^{2+} concentration; CTR, control.

and by the sarcolemma to maintain ion homeostasis (12–14) and hence a deficiency in glycolytic ATP could damage the integrity of cellular membranes. 2) Increasing flux through the PDC will prevent the accumulation of potentially toxic glycolytic end products such as lactate. 3) FA are known to have an "oxygen-wasting" effect when compared with carbohydrates, which results in a higher ratio between myocardial oxygen consumption and cardiac work. 4) Glucose utilization is necessary to supply ATP during increased cardiac output following β-adrenergic stimulation (10). Glucose and FA oxidation have a reciprocal relationship, described in a process known as the glucose/FA cycle (15). Increased levels of the FA oxidation intermediates acetyl-CoA, citrate, and NADH inhibit phosphofructokinase 1, the first and rate-limiting step in glycolysis (16). PDC is the second important key level of control regarding the use of glucose relative to FA for energy homeostasis. In addition to Ca^{2+}, PDC is regulated by various isoforms of pyruvate dehydrogenase kinase (PDK1, -2, -3, and -4) and phosphatase (PDP1 and -2), with phosphorylation inhibiting enzyme activity. Furthermore, products of FA oxidation (NADH and acetyl-CoA) activate PDKs resulting in PDC phosphorylation and inhibition (10).

Mitochondria accumulate Ca^{2+} from the cytosol in a tightly regulated way. In CM only 1–2% of cytosolic Ca^{2+} enters the MM during systole (17). $[Ca^{2+}]_m$ is regulated by a complex set of mechanisms influencing MM Ca^{2+} uptake and release, which have been reviewed (18, 19). Briefly, the outer MM is Ca^{2+} permeable (20), but import across the inner MM is highly regulated. The most important contributor to mitochondrial Ca^{2+} uptake is the mitochondrial Ca^{2+} uniporter (MCU) complex (MCUC) with the MCU serving as a highly selective channel that moves Ca^{2+} ions across the IMM dependent on the mitochondrial membrane potential ($\Delta\psi_m$) (21). Integrative genomics methods enabled the discovery of the molecular nature of the uniporter pore of MCU and its regulatory subunits: MCUb, EMRE, MICU1, MICU2, and MCUR1 (21–26). MCU is the pore-forming subunit of the MCU complex (21, 22). MCUb is the MCU paralog and behaves as a dominant-negative subunit affecting the Ca^{2+} permeation properties of the uniporter (25). High-affinity interaction of the MICU1-MICU2 complex with Ca^{2+} serves as an on–off switch, leading to a tightly controlled channel, capable of responding directly to cytosolic Ca^{2+} signals (23, 24, 27). EMRE is essential for the uniporter current and brackets the MCU pore and bridges the Ca^{2+}-sensing role of MICU1 and MICU2 with the Ca^{2+}-conducting role of MCU (26, 27). In the absence of EMRE, MCUC Ca^{2+} conductance does not occur (26). MCUR1 binds to MCU and EMRE and functions as a scaffold factor, thus being an important member of the MCUC (28).

Other mitochondrial Ca^{2+} import-linked proteins in the IMM have been identified (29, 30) although MCUC Ca^{2+} conductance is the dominant mechanism. CM mitochondrial Ca^{2+} export is mediated by the mitochondrial $Na^+/Ca^{2+}/Li^+$ exchanger (mNCLX) preventing mitochondrial Ca^{2+} overload (31). Short-term opening of the mitochondrial permeability transition pore also contributes to mitochondrial Ca^{2+} release (32).

During the systolic and diastolic phase of a heartbeat, inter-myofibrillar mitochondria, which are in close proximity to the SR, are exposed to the changing cytosolic Ca^{2+} concentration ($[Ca^{2+}]_i$) of the cytosolic Ca^{2+} transient. The CM-wide $[Ca^{2+}]_i$ increases from about 100 nM during diastole, to about 500 nM in systole; however, in the microdomain between the ryanodine receptor (RyR2) of the SR and the inter-myofibrillar mitochondria, $[Ca^{2+}]_i$ transiently rises to 10–20 μM during the systolic release phase of Ca^{2+} exiting the SR through the RyR2. Due to the relatively low affinity of MCU for Ca^{2+} the 20–40-fold higher $[Ca^{2+}]_i$ is required for mitochondrial Ca^{2+} uptake. This $[Ca^{2+}]_i$ persists for only about 10 ms during systole, which is the most active time for mitochondrial Ca^{2+} import by the MCUC (33). The mitochondrial Ca^{2+} transient follows the cytosolic Ca^{2+} transient with a slight delay, and a much smaller magnitude. The impact of mitochondrial Ca^{2+} handling is therefore not so much linked to its contribution to the cytosolic Ca^{2+} transients, but derives more from the important role of $[Ca^{2+}]_m$ stimulating mitochondrial respiratory function.

The significance of the MCU under *in vitro* hyperglycemic conditions was tested previously by us (34). Neonatal CM cultured in high glucose media showed decreased $[Ca^{2+}]_m$ due to decreased MCU protein levels. MCU transgene expression increased mitochondrial Ca^{2+} uptake, $[Ca^{2+}]_m$, PDC activity, and normalized fuel flux and protein *O*-GlcNAcylation with no detrimental effects. Furthermore, we demonstrated that MCU protein levels and $[Ca^{2+}]_m$ were reduced in hearts of diabetic mice.

Here we sought to investigate whether normalizing MCU levels *in vivo* in streptozotocin (STZ)-induced diabetic mice (annotated "DM" in the figures and table) restores mitochondrial Ca^{2+} handling, mitochondrial function, glucose oxidation, and cardiac function. In addition, we investigated deleterious effects of MCU expression in diabetic hearts. Our results show that restoring MCU toward the normal levels in murine diabetic hearts markedly improved mitochondrial Ca^{2+} handling, mitochondrial function, cardiac energetic metabolism, and subsequently both cardiac myocyte and heart function in the absence of adverse effects.

Results

Animal model

To ensure the efficacy of the STZ treatment, 8 weeks post-injection, and before experimental evaluation, mouse biometrics were analyzed and recorded (Table 1). We observed significantly lower heart (HW) and body weight (BW), whereas tibia length (TL) was not found different. Heart weight/body weight (HW/BW) ratios and heart weight/tibia length (HW/TL) ratios did significantly differ between control (CTR) and diabetic mice. Glucose tolerance measurements showed significantly higher levels in diabetic mice 1 h post-challenge (1.5 mg of glucose/g of BW) compared with controls, and fasting blood glucose levels were markedly increased in diabetic mice. Consistent with this model, insulin levels were below normal in diabetic mice. Neither thyroid hormone (triiodothyronine) dysregulation nor ketones were observed in diabetic mice. Finally, significantly elevated triglyceride levels were measured

Table 1
STZ-induced diabetic mouse model (DM) biometrics
Unpaired Student's *t* test for comparison between two groups was used.

	CTR	DM
Heart weight (mg)	124.85 ± 7.63	89.63 ± 5.51[a]
Body weight (g)	34.75 ± 2.97	20.15 ± 2.27[a]
Tibia length (cm)	1.79 ± 0.04	1.76 ± 0.04 (NS)[b]
Heart weight/body weight (mg/g)	3.71 ± 0.12	4.46 ± 0.21[a]
Heart weight/tibia length (mg/cm)	0.70 ± 0.004	0.51 ± 0.004[a]
Blood glucose, 1 h post-challenge (mg/dl)	153.8 ± 8.23	>600[c]
Fasting blood glucose (mg/dl)	72.3 ± 7.20	396.0 ± 51.0[c]
Insulin (ng/ml)	100.4 ± 33.7	32.7 ± 12.3[c]
Triiodothyronine (ng/dl)	93.3 ± 29.7	108.0 ± 26.9 (NS)
Ketones	Negative	Negative
Total cholesterol	102.25 ± 7.80	102.5 ± 18.34 (NS)
Triglycerides	83 ± 31.56	228 ± 81.61[c]

[a] $p < 0.001$. Data are representative of 6 mice per group and are presented as mean ± S.D.
[b] NS, not significant.
[c] $p < 0.05$. Data are representative of 6 mice per group and are presented as mean ± S.D.

in plasma from diabetic *versus* CTR mice, whereas cholesterol levels were unchanged (Table 1).

MCU and MCUC member levels are altered in diabetic hearts

MCU and MCUC member protein levels were determined in hearts of diabetic and control mice. As shown in Fig. 1, MCU protein levels were decreased by 50% in diabetic hearts 8 weeks post-STZ, compared with control hearts (Fig. 1*A*). Moreover, at 26 weeks we observed that MCU protein levels had decreased by 70% from control levels (Fig. 1*A*). We also determined MCU mRNA levels in 8-week-old diabetic mice by RT-qPCR and observed a 50% decrease, in line with the protein decay (Fig. 1*B*). Therefore, further studies were conducted using 8-week-old diabetic mice. Western blot analysis of other MCUC members in the 8-week diabetic heart also showed that EMRE was significantly decreased by 36%. In contrast, MCUb protein levels were increased by 31% with no significant change for MICU1, MICU2, and MCUR1 (Fig. 1*C*).

Adeno-associated virus-MCU (AAV-MCU) expression

To restore MCU protein levels toward normal, an adeno-associated viral vector carrying the complete coding sequence of the murine MCU mRNA (AAV-MCU) was generated in the liver-detargeted, cardiac-preferred serotype 9 variant, 9.45 (35). Cardiac-preferred MCU expression was confirmed by Western blotting in several organs from control, 3-month-old mice (Fig. 2, *A* and *B*). To ensure correct evaluation of tissue specificity mice were injected with higher AAV doses (1×10^{12} genome copies). Even though intramuscular injection (IM) of AAV-MCU was found to induce MCU expression in skeletal muscle, the jugular vein delivery approach used for this study was able to induce AAV accumulation and consequently expression only in heart. Subsequently, MCU restoration was attempted in diabetic mice. AAV-MCU was injected through the jugular vein and after 4 weeks we observed a complete MCU restoration (Fig. 2*C*) instead of MCU overexpression as in Fig. 2, *A* and *B*, due to the lower AAV titer used in these experiments (3×10^{11} *versus* 1×10^{12} genome copies). As control an empty AAV (AAV-empty) was injected. No effect of AAV-empty was observed, as reported by others (36). In the hearts of AAV-MCU-treated mice we measured $8.3 \pm 1.1 \times 10^5$ AAV vector genome copy numbers per μg of genomic DNA.

MCU expression restores mitochondrial Ca^{2+} handling, mitochondrial bioenergetics, and reverses energetic metabolism in diabetic mice

The effects of MCU restoration on mitochondrial Ca^{2+} handling were evaluated in isolated CM from CTR, diabetic, and from hearts of diabetic mice receiving AAV-MCU. All mice received AAV expressing the mitochondrial Ca^{2+} sensors Mitycam or MitoPericam (Fig. 3). Mitochondrial Ca^{2+} uptake and release rates, and $[Ca^{2+}]_m$ were assessed in isolated, fluorescent, rod-shaped cells responding to electric stimulation (pacing frequency = 0.3 Hz). Mitochondrial Ca^{2+} uptake and release were assessed using Mitycam. CM from hearts of diabetic mice showed markedly reduced mitochondrial Ca^{2+} transients with significantly lower uptake rate and slightly lower release rate compared with control, whereas MCU restoration rectified these measurements (Fig. 3*A*). Furthermore, $[Ca^{2+}]_m$ in paced-contracting CM (Fig. 3*B*) and the mitochondrial matrix-free Ca^{2+} content in permeabilized CM (Fig. 3*C*) were consistently decreased in diabetic CM compared with controls. $[Ca^{2+}]_m$ and the mitochondrial matrix-free Ca^{2+} content were restored toward control values after MCU expression (Fig. 3, *B* and *C*).

$[Ca^{2+}]_m$ plays a central role in controlling the rate of activation of the tricarboxylic acid cycle dehydrogenases and is an important regulator of electron transport chain-mediated ATP production by stimulating different mitochondrial complexes and dehydrogenases during oxidative phosphorylation (5). Therefore, we evaluated the potential beneficial effects arising from improved mitochondrial Ca^{2+} handling following MCU restoration in diabetic hearts.

The PDC activity was dramatically reduced in hearts from diabetic mice. MCU expression in diabetic mice significantly improved PDC activity (Fig. 4*A*). These results were consistent with a higher level of phosphorylated PDC protein in diabetic hearts that was reduced after MCU expression (Fig. 4*B*). Due to the importance of PDC as a key regulator of glucose and FA oxidation, we investigated whether the reduced PDC phosphorylation and increased PDC activity following MCU expression could have an impact on cardiac metabolism. To this end glucose and FA oxidation were measured in working heart preparations (Fig. 4*C*). We observed in diabetic hearts that the rates of mitochondria-mediated glucose oxidation and palmitate oxidation were significantly reduced and increased, respectively. Interestingly, diabetic hearts expressing transgenic MCU showed completely reversed profiles where glucose oxidation increased and FA oxidation showed a reciprocal decrease, both to control levels.

A metabolic shift was also observed in metabolomics studies. Plasma and hearts samples from CTR, diabetic, and diabetic mice transduced with AAV-MCU were analyzed. Metabolites that showed significant differences between CTR and diabetic mice were plotted across all three groups for both plasma and heart samples (Fig. 5*A*). In plasma, widespread changes with diabetes were observed, and MCU transgene expression had little effect as demonstrated by hierarchical clustering. In con-

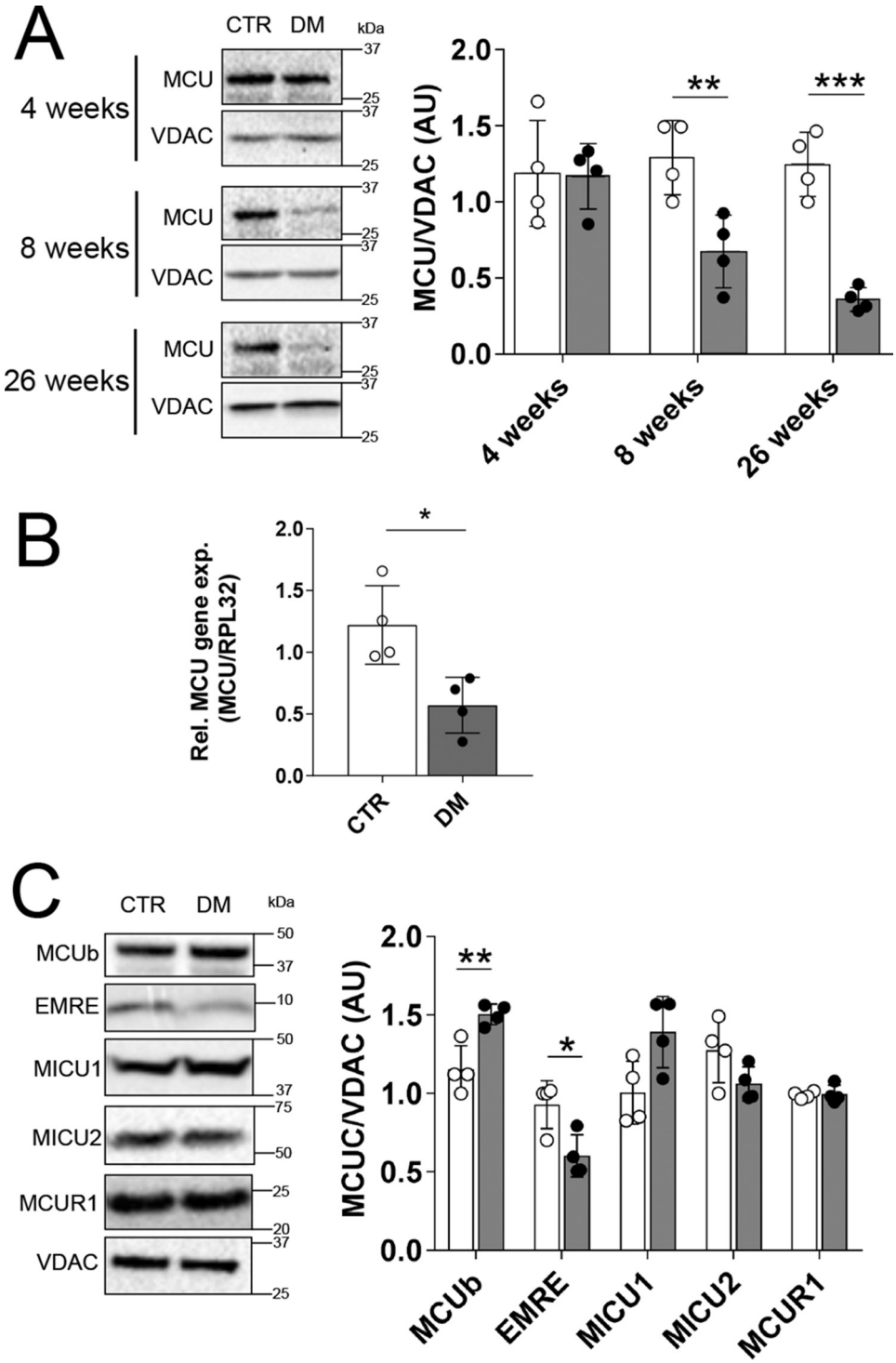

Figure 1. MCU protein levels with progression of diabetes, MCU mRNA, and MCUC protein levels at 8 weeks post-STZ injection. *A*, Western blot analysis of MCU protein levels in hearts of control (*CTR, white bars*) and diabetic (*DM, gray bars*) mice at 4, 8, and 26 weeks of diabetes (*left*). Summarized data of densitometric band analysis are shown (*right*). MCU levels were normalized by the mitochondrial voltage-dependent anion channel (*VDAC*). *B*, RT-qPCR analysis of MCU mRNA levels in CTR and DM mouse hearts at 8 weeks of diabetes. 60S ribosomal protein L32 (RPL32) was used as the housekeeping gene for normalization. *C*, Western blot analysis of other MCUC members: MCUb, EMRE, MICU1, MICU2, and MCUR1 (*left*). Summarized data of densitometric band analysis are shown (*right*). MCUC member levels were normalized by VDAC expression. All data are representative of 4 animals per group and presented as mean ± S.D. Unpaired Student's *t* test for comparison between two groups was used. *, $p < 0.05$; **, $p < 0.01$; ***, $p < 0.001$.

trast to plasma, hierarchical clustering of metabolites in heart samples demonstrated that MCU transgene expression reverted the diabetes-induced changes in a large number of metabolites. We then measured the levels of glucose in the plasma and heart from the same group of mice by LC-MS/MS analysis (Fig. 5*B*). Consistent with the decreased glucose oxidation measured in working heart preparations and with the diabetic mouse model, higher levels of glucose were measured in both plasma and heart from diabetic mice. MCU transgene expression in the hearts of these mice significantly reduced glucose levels in the

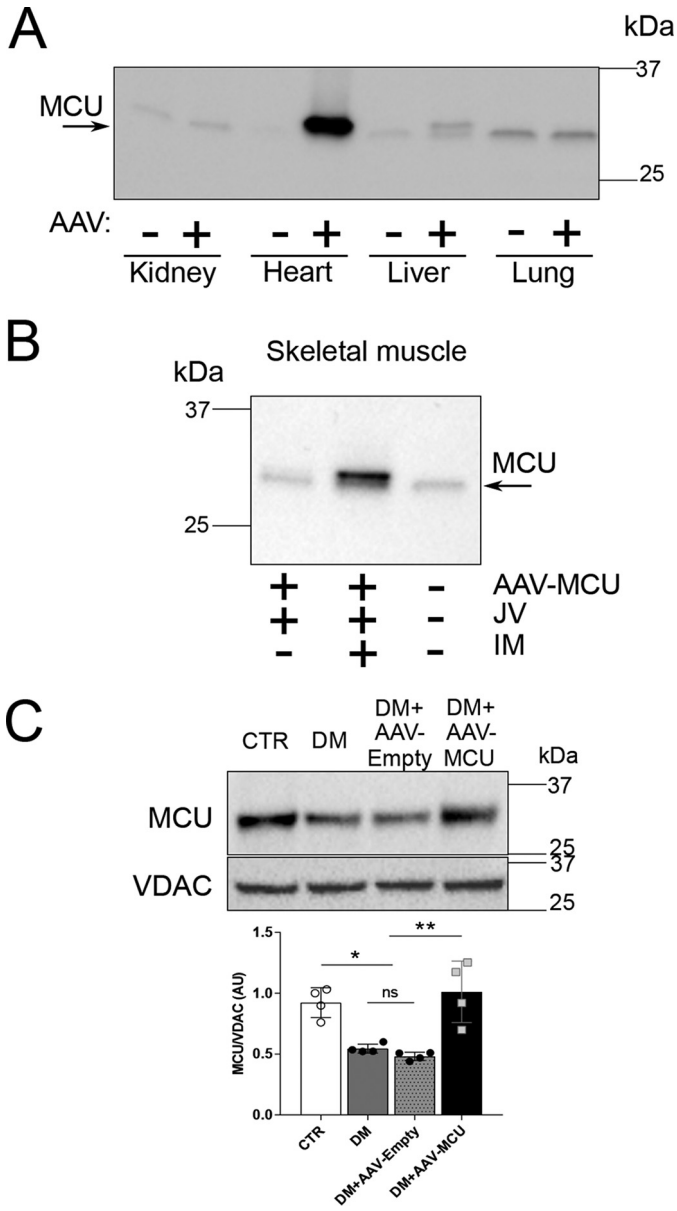

Figure 2. *In vivo* preferential cardiac MCU expression is obtained with adeno-associated virus 9.45 carrying the MCU cDNA sequence (AAV-MCU), and is used to restore MCU protein levels in STZ-induced diabetic mouse hearts. *A,* representative Western blotting showing MCU levels 4 weeks after AAV-MCU delivery by jugular vein. MCU levels were measured in kidney, heart, liver, and lung cardiac-preferred and liver-reduced MCU expression was observed. *B,* skeletal muscle MCU transgene expression is obtained only with IM AAV injection and not with jugular vein (*JV*) injection. In *A* and *B* a higher titer was used to ensure correct evaluation of AAV tissue specificity (1×10^{12} genome copies). *C,* Western blotting showing MCU restoration in 8-week diabetic mouse hearts 4 weeks after AAV-MCU injection (*top*). No significant increase was observed with delivery by jugular vein of empty AAV particles (*AAV-empty*). Summarized data of densitometric band analysis are shown (*bottom*). Data are representative of 4 animals per group and are presented as mean ± S.D. One way ANOVA with Tukey's multiple comparisons test was used. *, $p < 0.05$; **, $p < 0.01$.

heart, but not in plasma, confirming the cardiac specificity of the transgenic therapeutic intervention and suggesting a direct link between restored mitochondrial Ca^{2+} handling and normalized oxidative metabolism.

MCU protein restoration also positively influenced mitochondrial respiration and functionality. The respiratory control ratio (RCR) (state 3/state 4) was found to be lower in isolated mitochondria from diabetic hearts compared with control (Fig. 6*A*), and MCU expression rectified RCR toward control values (Fig. 6*A*). Furthermore, $\Delta\psi_m$ measured in isolated CM from diabetic mice was decreased by 40% and was returned toward normal levels in CM from diabetic mice after MCU expression (Fig. 6*B*). In addition, ATP production in isolated mitochondria assessed by the 2-deoxy-D-glucose (2DG) ATP energy clamp method (37) demonstrated that reduced ATP production in mitochondria from diabetic hearts was increased after MCU expression, despite persistent diabetes (Fig. 6*C*).

Cardiac function in diabetes is improved by MCU expression

The effect of MCU rectification on CM contractility was analyzed with the edge detection technique. A decreased rate of cell shortening/contraction (+dL/dt), rate of re-lengthening (−dL/dt), and fractional cell shortening was observed in CM from diabetic mice, compared with control CM, and an improvement in CM from diabetic mice treated with AAV-MCU is shown in Fig. 6. +dL/dt and −dL/dt were increased by 28 and 74% (Fig. 7, *A* and *B*), respectively, in CM from diabetic mice treated with AAV-MCU, compared with CM from diabetic mice. Moreover, rectification of MCU levels improved fractional cell shortening by 86% (Fig. 7*C*). Subsequently, cardiac contractility was assessed *ex vivo* in isolated-perfused hearts. Diminished rates of contraction (+dP/dt) and relaxation (−dP/dt) in diabetic hearts were observed and MCU transgene expression returned these parameters toward normal (Fig. 7, *D* and *E*). *In vivo* cardiac performance was ultimately evaluated by echocardiography and AAV-MCU-treated diabetic mice showed fractional shortening returned toward control values, despite persistent diabetes (Fig. 7*F*).

Restoration of normal MCU levels reduces apoptosis, protein oxidation, and cardiac infarct size

Given the role of mitochondrial Ca^{2+} overload on a variety of processes leading to oxidative stress and cell death, we explored potential, unintended negative effects related to MCU restoration in diabetes (Fig. 8). Apoptosis was assessed by Western blot analysis of activated cleaved caspase 3 (Fig. 8*A*). The results showed that increased cleavage of caspase 3 in diabetic hearts was reduced toward control levels in the hearts of diabetic mice treated with AAV-MCU. Moreover, oxidation of total proteins extracted from whole hearts clearly showed diminished oxidation in AAV-MCU-treated diabetic samples (Fig. 8*B*). In addition, myocardial infarct size was evaluated in isolated-perfused hearts in which global ischemia/reperfusion was induced. Diabetic hearts showed an infarcted area 3.2-fold larger than in control mice. In contrast, hearts from diabetic mice treated with AAV-MCU showed a significant reduction in the infarcted area (2.2-fold *versus* CTR) (Fig. 8*C*).

Discussion

We report here for the first time that *in vivo* AAV-based MCU transgene expression in the CM of diabetic mouse hearts had beneficial effects on mitochondrial Ca^{2+} handling, PDC activity, oxidative phosphorylation substrate utilization, mitochondrial respiration, $\Delta\psi_m$, and ATP production, despite per-

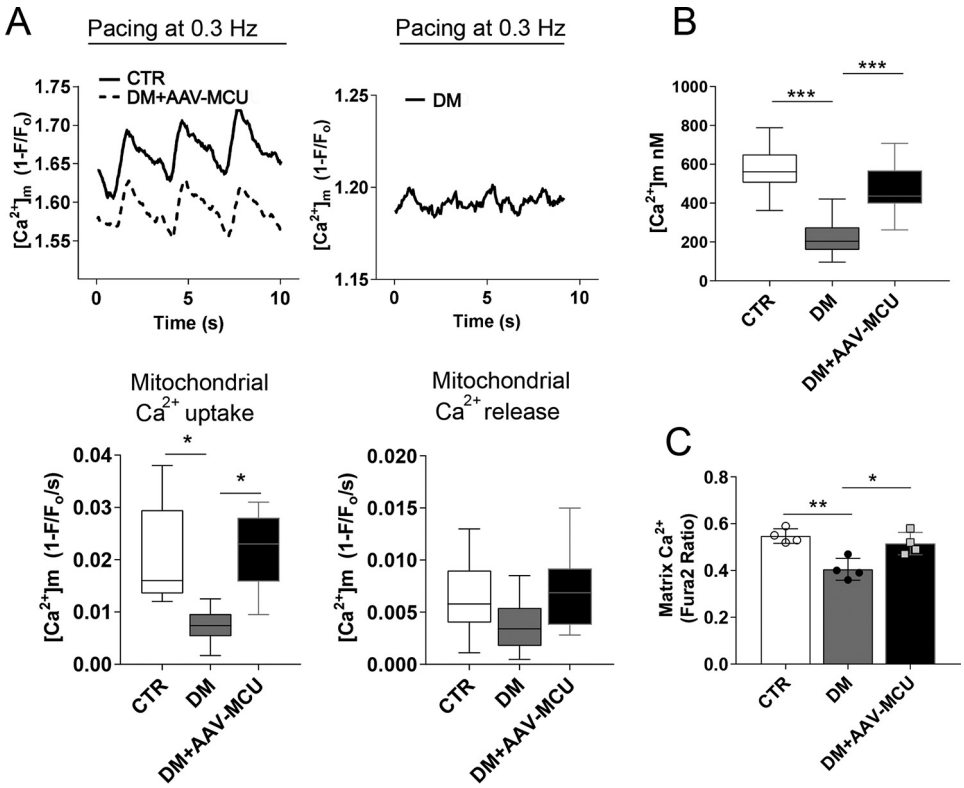

Figure 3. Impaired mitochondrial Ca^{2+} handling in diabetic CM is significantly improved by MCU restoration. *A,* representative mitochondrial Ca^{2+} transients measured in isolated CM from CTR, DM, and DM + AAV-MCU mouse hearts (*top*). Mitochondrial Ca^{2+} transients were assessed in paced-contracting CM (0.3Hz) using Mitycam, which was delivered *in vivo* by injection of AAV-Mitycam at the same time as AAV-MCU. Mitochondrial Ca^{2+} uptake and release rates were quantified and are shown in the graph (*bottom*). Data are representative of recordings from $n \geq 10$ cells isolated from 4 mice per group. *B,* mitochondrial Ca^{2+} level ($[Ca^{2+}]_m$ at peak) in intact paced-contracting CM was assessed using MitoPericam (AAV-MitoPericam and AAV-MCU were injected simultaneously). CM were paced at 0.3 Hz. Data are representative of recordings from $n \geq 70$ cells from 4 mice for each group. *C,* matrix Ca^{2+} content in isolated and permeabilized CM was assessed with Fura-2. Isolated CM were permeabilized with digitonin and incubated with thapsigargin (SERCA inhibitor), CGP-37157 (mNCLX inhibitor), and Ru360 (MCU inhibitor). $[Ca^{2+}]_m$ was released from the MM with FCCP. Data are representative of CM isolated from 4 animals per group. All data are presented as mean ± S.D. One-way ANOVA with Tukey's multiple comparisons test was used. *, $p < 0.05$; **, $p < 0.01$; ***, $p < 0.001$.

sistent diabetes. These beneficial effects were associated with improved cardiac performance of the heart both *ex vivo*, in the isolated CM and Langendorff-perfused heart, and *in vivo*. No detrimental effects from MCU restoration in diabetic hearts were observed. This experimental evidence was obtained using an STZ-induced diabetic mouse model that shares clinically important features with human type 1 diabetes. Indeed, STZ-treated animals have been used to study diabetogenic mechanisms and for preclinical evaluation of novel anti-diabetic therapies. Although the etiopathology of diabetes in humans is largely dependent by an autoimmune mechanism the diabetes in our mouse model is chemically induced by STZ. However, diabetic cardiomyopathy can successively be achieved in STZ-induced diabetic mice so our results provide the basis for further studies that could be performed in the human heart.

Mitochondrial Ca^{2+} uptake is achieved primarily through the MCUC, which consists of a pore-forming protein MCU. The MCU pore is a highly selective Ca^{2+} channel that moves Ca^{2+} ions across the IMM, and interacts with its regulatory and structural subunits: MCUb, MICU1, MICU2, MCUR1, and EMRE.

Recently, the pathophysiological role of MCUC in diabetes has become a topic of investigation. We previously reported that MCU protein levels and $[Ca^{2+}]_m$ were decreased in diabetic mice (34), and have confirmed these results here. In addition, we observed diminished mitochondrial Ca^{2+} uptake and mitochondrial Ca^{2+} content in diabetic CM. Regulatory members of the MCUC such as MCUb and EMRE were also influenced by diabetes. Surprisingly, we did not observe significant changes in MICU1, which was found down-regulated in the hearts of the Leptin receptor-deficient (*db/db*) C57BLKS diabetic mouse model (38). The same report showed no changes to MCU levels in 12-week-old *db*/*db* mouse hearts although lower MCU protein levels can be observed in their Western blotting results at 18 weeks of age (38). Differences between our diabetic model and the *db/db* diabetic mouse model may be expected because STZ-induced diabetic mice have very low insulin levels in contrast to the *db*/*db* diabetic model mice, which display hyperinsulinemia (39). In addition, in *db*/*db* mice signaling by the leptin receptor is abnormal (40). It is interesting to note that different diabetic models result in specific changes of MCUC members. This necessitated varying rescue efforts focusing on different MCUC members.

Our findings show decreased MCU protein levels, corresponding to reduced MCU mRNA levels (−50%). Hyperglycemia may be a contributing factor to MCU down-regulation in a STZ-induced diabetic model because we have previously demonstrated that exposing cultured neonatal CM to hyperglycemia leads to markedly decreased MCU levels (34).

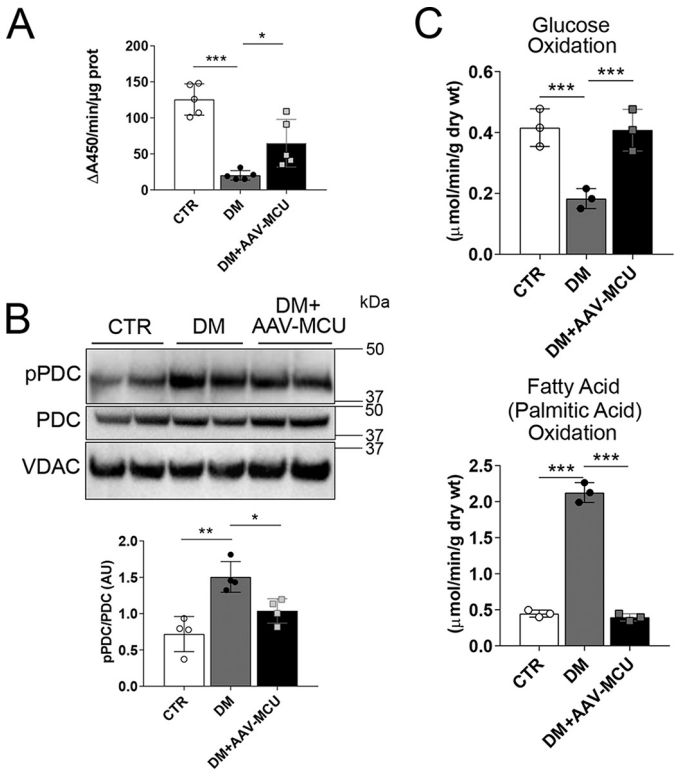

Figure 4. MCU transgene expression increases PDC activity by reducing PDC phosphorylation thereby inducing a metabolic oxidation switch. *A,* PDC activity was measured in total heart lysates using a microplate assay kit following the reduction of NAD^+, coupled to the reduction of a reporter dye (450 nm). Data were normalized over total protein content and are representative of 5 total mouse heart lysates. *B,* Western blot analysis of PDC phosphorylation (*pPDC*) levels (*top*) representative of 4 animals. Total PDC protein levels were not changed and used for normalization. Total PDC levels were normalized over VDAC levels. Summarized densitometric band analysis are shown (*bottom*). *C,* glucose and palmitic acid were used to measure glucose and fatty acid oxidation in working heart preparations. Substrate oxidation is reported as micromole/min/g dry weight. All data are presented as mean ± S.D. One-way ANOVA with Tukey's multiple comparisons test was used. *, $p < 0.05$; **, $p < 0.01$; ***, $p < 0.001$.

Our results and prior findings (2–4, 34, 38) strongly suggest a link between dysfunctional mitochondrial Ca^{2+} handling and impaired cardiac function in diabetes. In this report we further investigated whether restoring mitochondrial Ca^{2+} handling in diabetic hearts could have beneficial effects on cardiac metabolism and function, despite persistent diabetes.

In vivo AAV-mediated MCU expression in the hearts of diabetic mice restored MCU protein levels and Ca^{2+} handling. $[Ca^{2+}]_m$ enhances oxidative phosphorylation leading to enhanced ATP formation (5). In addition, several dehydrogenases in the MM are activated by $[Ca^{2+}]_m$, including PDC (6, 7). Accordingly, our results show that restoring mitochondrial Ca^{2+} handling in diabetic hearts leads to positive downstream Ca^{2+}-dependent effects. By rectifying $[Ca^{2+}]_m$, normalized allosteric regulation by Ca^{2+} of several mitochondrial respiratory chain complexes is likely the reason why we observed restoration of mitochondrial respiration, which enhances ATP production and $\Delta\psi_m$. Furthermore, restored $[Ca^{2+}]_m$ might either directly stimulate PDC activity or influence it by activation of Ca^{2+}-dependent mitochondrial phosphatases (6, 7). Consequently, the shift from FA to glucose oxidation observed both in the working heart preparation and with metabolomics studies is possibly mediated by the higher PDC activity in diabetic mice with MCU restoration.

Improving mitochondrial function also resulted in improved CM contractility, *ex vivo* cardiac contraction, and *in vivo* fractional shortening. Based on the data presented in this report, and consistent with a model in which cardiac metabolic substrates utilization is normalized, the observed increase in contractile function can be viewed as a consequence of a more efficient metabolism resulting from improved mitochondrial Ca^{2+} handling. Our results are in agreement with findings from Ji *et al.* (38). These authors overexpressed MICU1 in a db/db diabetic mouse model resulting in alleviated diabetic cardiomyopathy by an antioxidant mechanism. MICU1 regulates the MCUC and potentially could improve mitochondrial Ca^{2+} handling, but detailed analysis of mitochondrial Ca^{2+} handling was not provided (38).

In heart failure that is linked to myocardial ischemia mitochondrial Ca^{2+} overload can occur, triggering mitochondrial permeability transition pore opening and leading to CM death (41). To assure that no detrimental consequences result from MCU restoration in diabetes, where mitochondrial $[Ca^{2+}]$ is restored toward normal, we determined CM death and myocardial infarct size in diabetic mice and in diabetic mice with AAV-MCU expression. Our findings show that MCU expression did not increase the infarcted area after global ischemia/reperfusion in the diabetic heart. On the contrary, the infarcted area was reduced in diabetic heart when MCU was expressed. Improved mitochondrial respiratory function and ATP formation as a consequence of increased glucose utilization may explain the better recovery of cardiac myocytes upon ischemia/reperfusion injury (42). These results also correlate with the reduction in cleaved caspase 3 in diabetic heart with MCU expression. In addition, increased protein oxidation in the diabetic heart was reduced by MCU expression. All together these data indicate that MCU restoration in the diabetic heart does not trigger detrimental effects nor worsen Ca^{2+} overload-induced damage.

Only recently have the molecular components of the MCUC been identified (21–26). The physiological and pathological relevance of the MCUC are actively investigated. The physiological role of MCU is currently debated, in response to data obtained in MCU KO models (43). For instance, early results from MCU KO models showed a very mild cardiac phenotype unless acutely challenged (43). However, recent data from new KO models for MCU produced by the International Mouse Phenotype Consortium (IMPC) showed that ablation of MCU (that completely blocks mitochondrial Ca^{2+} uptake) leads to embryonic lethality, and MCU+/− heterozygous mice show several impaired physiological functions including decreased cardiac stroke volume (reviewed in Ref. 44). The paradoxical function of MCU observed in the various MCU KO models may be due to compensatory effects, alternative Ca^{2+} import mechanisms, genetic background, or the techniques used to make the models. Currently no reports have addressed the influence of MCU in chronically stressed and challenged models such as the STZ-induced diabetic mouse. Our data demonstrate for the first time that restoring MCU protein levels in the diabetic heart promotes beneficial effects, suggesting a key role of

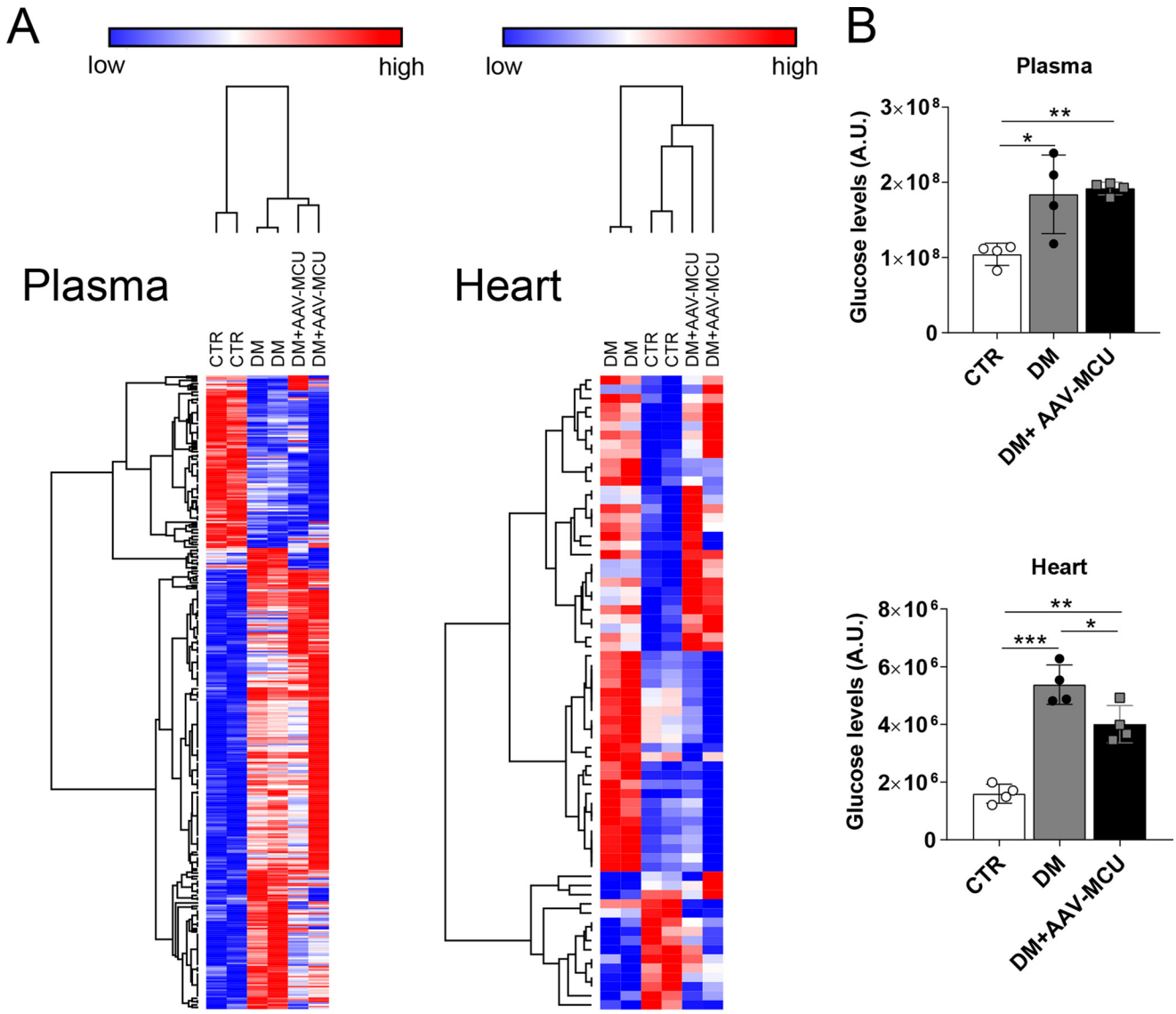

Figure 5. Metabolomics analysis confirms the global cardiac-specific effect of AAV-MCU in diabetic mice. *A,* metabolomics analysis was conducted in plasma and heart, and metabolites that differed significantly were used to generate heat maps. Hierarchical clustering was obtained using Spearman rank correlation. Each row represents one metabolite characterized by specific molecular mass. A color gradient was introduced to visualize relative metabolite levels (*blue* = low levels, *red* = high levels). MCU transgene expression shifted the metabolomics profile toward CTR only in the heart as evidenced by hierarchical clustering. *B,* glucose levels in heart and plasma samples (glucose is reported in arbitrary units, *AU*). All data are presented as mean ± S.D. One-way ANOVA with Tukey's multiple comparisons test was used. *, $p < 0.05$; **, $p < 0.01$; ***, $p < 0.001$.

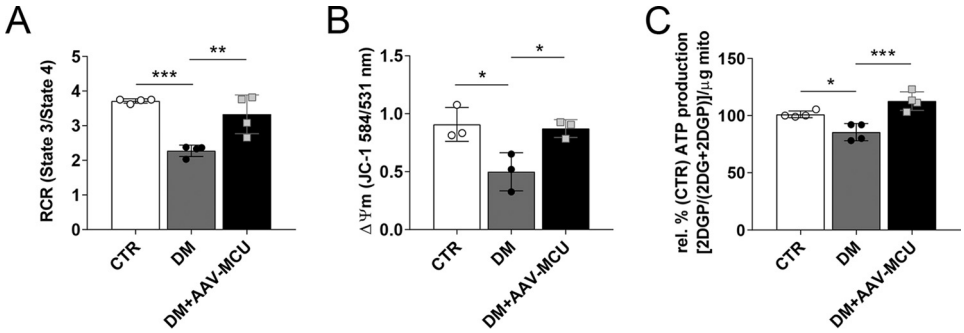

Figure 6. MCU expression improves mitochondrial respiratory dysfunction in diabetic hearts. *A,* mitochondrial respiration was measured by Clark electrode and the RCR was calculated according to procedures described under "Experimental procedures." Data are representative of cardiac mitochondria isolated from 4 mouse hearts per group. *B,* mitochondrial transmembrane potential ($\Delta\psi_m$) was evaluated as the ratio of JC-1 fluorescence at 584/531 nm. Fluorescence emission was collected from isolated CM. Data are representative of at least 30 individual cell recordings from 3 mice for each group. *C,* rates of mitochondrial ATP production measured in mitochondria isolated from 4 mice per group. ATP production is reported as percentage of phosphorylated 2DG (*2DGP*) over total 2DG obtained in a 20-min reaction. Data are relative to rates registered in mitochondria from control mice and are normalized per μg of mitochondria. All data are presented as mean ± S.D. One-way ANOVA with Tukey's multiple comparisons test was used. *, $p < 0.05$; **, $p < 0.01$; ***, $p < 0.001$.

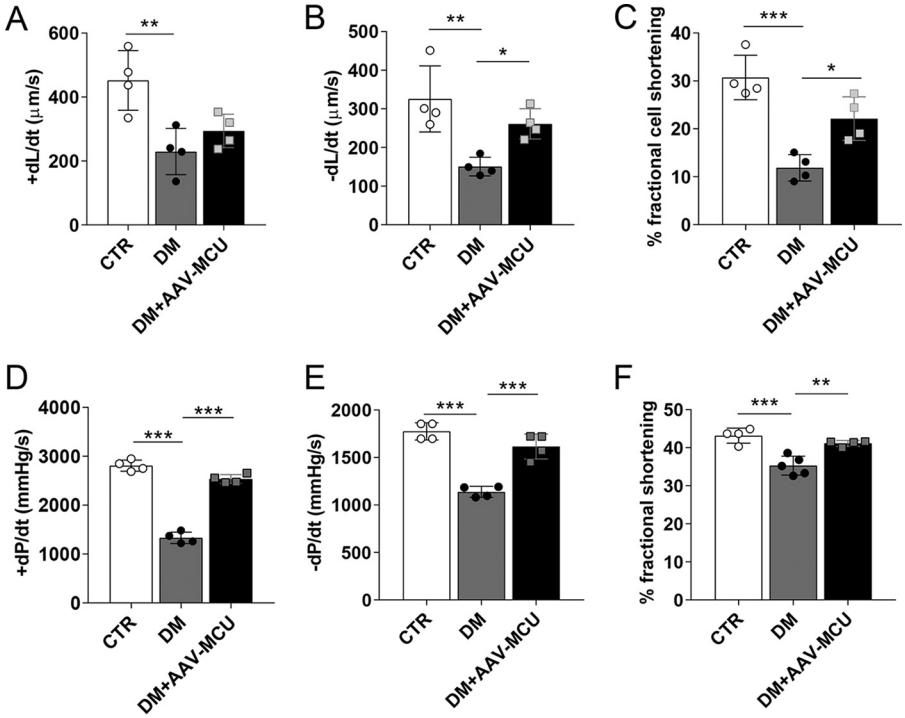

Figure 7. MCU expression improves CM contractility and both *ex vivo* and *in vivo* contractile function. CM contractility was assessed by edge detection and cell shortening is shown. *A,* rate of contraction (+dL/dt) was similar in DM *versus* (*versus*) DM + AAV-MCU. *B,* rate of relaxation (−dL/dt) and *C,* % fractional cell shortening were significantly improved in DM + AAV-MCU *versus* DM. Heart function was assessed *ex vivo* using Langendorff-perfused heart preparations. Hearts were paced at 400 bpm and the resulting pressure waves were recorded and analyzed. Summarized data are related to *D,* +dP/dt max and *E,* −dP/dt min are shown and demonstrate a significant improvement in DM + AAV-MCU *versus* DM hearts. *F, in vivo* heart function was assessed by M-mode echocardiography and a significantly increased % fractional shortening is shown in DM + AAV-MCU *versus* DM hearts. All data are representative of 4 animals and are presented as mean ± S.D. One-way ANOVA with Tukey's multiple comparisons test was used. *, $p < 0.05$; **, $p < 0.01$; ***, $p < 0.001$.

MCUC in the pathophysiology leading to diabetes-mediated decreased cardiac function.

In conclusion, restoring MCU levels in diabetic hearts improves both CM and heart metabolism and function by rectifying the abnormal mitochondrial Ca^{2+} handling associated with diabetic cardiac disease without any detrimental effects. Therefore, mitochondrial Ca^{2+} handling can be considered a suitable therapeutic target in diabetes-related cardiac disease.

Experimental procedures

Animals

All investigations conformed to the Guide for the Care and Use of Laboratory Animals published by the National Institutes of Health (NIH Publication No. 85-23, revised 1985). This study was conducted in accordance with the guidelines established by the Institutional Animal Care and Use Committee at the University of California, San Diego.

Diabetic mouse model

Diabetes was induced in C57BL/6NHsd mice (25 g, 3 months old) by giving a daily intraperitoneal injection of STZ (40 mg/kg) for five consecutive days, as previously described (45). Diabetes onset was documented by measuring blood glucose above 250 mg/dl. These mice were nonketotic and euthyroid, as previously reported (46). Total cholesterol and triglycerides were measured by the UCSD Mouse Phenotyping Service according to standard procedures.

AAV administration

In vivo AAV transgene delivery was performed by direct jugular vein injection of liver-detargeted, double-stranded AAV serotype 9.45 particles produced by the UCSD Vector Development Core Laboratory (47). Empty AAV (AAV-Empty) or AAV encoding C-terminal FLAG-tagged murine MCU (AAV-MCU), mitochondria-localized ratiometric-pericam (AAV-MitoPericam), or Mitycam (AAV-Mitycam) was injected 8 weeks after injection with STZ (3×10^{11} genome copies for AAV-MCU, 7×10^{11} genome copies for AAV-MitoPericam and AAV-Mitycam, in 100 μl). Experiments were carried out 8–10 weeks after STZ injection, and 4–6 weeks after AAV-MCU delivery.

Determination of AAV vector genome copy number

Approximately 15 mg of tissue from the apex of the heart was processed using the PureLink Genomic DNA Mini Kit (Life Technologies). Vector genome copy numbers were determined by qPCR using DyNAmo ColorFlash SYBR Green (Thermo) and an Agilent Mx3005P cycler. Primers specific for the FLAG-tagged MCU transgene were used for amplification (forward, 5′-AGGAGCCAAAAAGTCACGTTTC; reverse 5′-CTTATC GTCGTCATCCTTGTAATC). A standard curve was created using known copy numbers of plasmid DNA containing the transgene construct. Results are expressed as the vector copy number per microgram of genomic DNA as described (48).

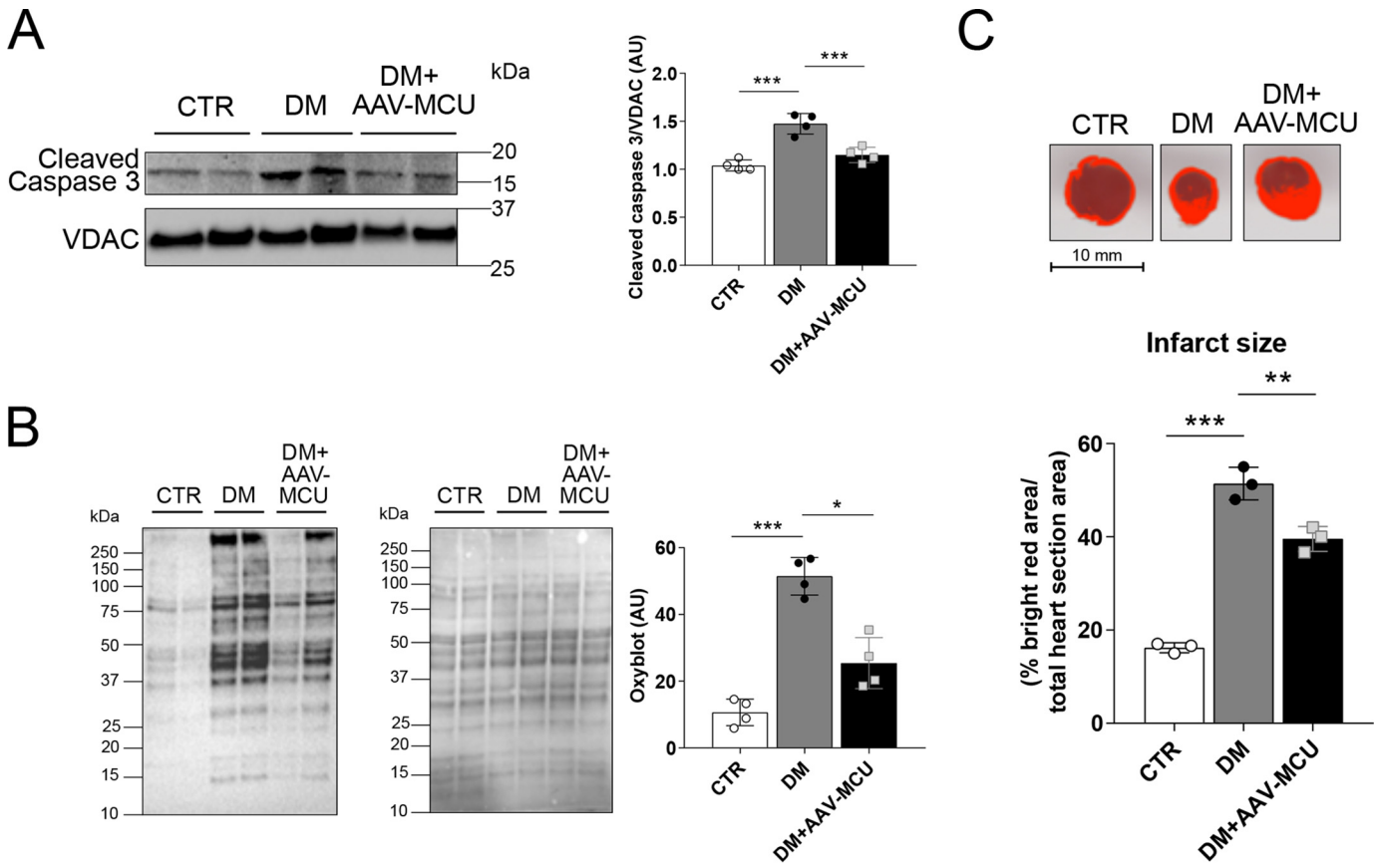

Figure 8. MCU expression reverts caspase 3 activation and protein oxidation in diabetic hearts and does not increase ischemia/reperfusion damage. *A,* Western blot analysis of cleaved (activated) caspase 3 as a general marker of apoptosis (*left*). VDAC was used as protein loading control. Summarized densitometric band analysis is shown (*right*). Data are representative of total heart protein lysates from 4 animals per group. *B,* Western blot analysis of total protein oxidation (*left*) as marker of oxidative stress in heart lysates. Polyvinylidene difluoride membranes were stained for total protein as loading control. Summarized densitometric band analysis is shown (*right*). Data are representative of 4 animals per group. *C,* influence of MCU expression on mouse heart infarct size following global ischemia/reperfusion. Following ischemia/reperfusion, hearts were sectioned and photographed. The infarcted area is highlighted in *bright red* around the perimeter of the section using ImageJ (*top*). *Dark red* represents viable tissue. Infarct size (% infarcted area over total area) was calculated and is reported (*bottom*). The experiment was performed on 3 hearts per group. All data are presented as mean ± S.D. One-way ANOVA with Tukey's multiple comparisons test was used. *, $p < 0.05$; **, $p < 0.01$; ***, $p < 0.001$.

Isolation of CM

Ca^{2+} tolerant adult CM were isolated from ventricular tissue by a standard enzymatic digestion procedure described previously (49). CM were cultured on glass coverslips coated with laminin.

Mitochondria preparation

Mitochondria were isolated as previously described (45). To ensure mitochondrial viability for ATP production and O_2 consumption assays all steps were performed at 4 °C.

Langendorff-perfused hearts and global ischemia/reperfusion protocol

Heart function was assessed *ex vivo* as previously described by us (50, 51). Pressure development was recorded digitally (1 kHz) by connecting the intraventricular balloon to a 2-F Millar pressure transducer. The hearts were paced at 400 bpm and the resulting pressure waves were analyzed for pressure derivatives (+dP/dt, −dP/dt) and pressure development. Global ischemia/reperfusion experiments were performed as described previously (52). Hearts were allowed to stabilize for 30 min and subsequently, perfusion flow was stopped for 15 min followed by 60 min reperfusion. Hearts were frozen and cut into 6–8 transverse slices from apex to base of equal thickness (1 mm). Heart slices were stained with 10% tetrazolium chloride for 30 min and infarct size was determined by computer morphometry using ImageJ software.

Transthoracic M-mode echocardiography

Cardiac echography was performed on lightly anesthetized mice using a FUJIFILM Visualsonics Vevo 2100 ultrasound system, as described (53).

Measurement of CM contractility by edge detection

The edge detection of cultured adult CM was performed according to the method described (49).

Western blotting

Protein levels were assessed by Western blot analysis as previously described (45). 50–100 μg of protein samples were loaded on NuPAGE 4–12% BisTris gels (Invitrogen). Separated proteins were transferred to polyvinylidene difluoride membranes. Anti-MCU (Sigma, HPA016480; 1:1000), anti-MCUb (Sigma, HPA048776; 1:500), anti-EMRE (Santa

Cruz, SC-86337; 1:200), anti-MICU1 (Sigma, HPA037480; 1:1000), anti-MICU2 (Abcam, ab101465; 1:1000), anti-MCUR1 (Cell Signaling, 13706; 1:1000), anti-cleaved Caspase 3 (Cell Signaling, 9661S; 1:200), anti-PDC (Cell Signaling, 2784; 1:1000), anti-PDC E1-α subunit (phosphor-Ser-293) (Abcam, ab92696; 1:1000), and anti-VDAC (Cell Signaling, 4866; 1:500) were used as primary antibodies. Anti-mouse IgG-horseradish peroxidase-conjugated (ThermoFisher Scientific 31430; 1:5000) and anti-rabbit IgG–horseradish peroxidase-conjugated (Cell Signaling, 7074; 1:5000) were used as secondary antibodies. Images were acquired on film or with the Chemi-Doc MP System (Bio-Rad). Band density was quantified with ImageJ software as previously described (54). VDAC was used as loading control for Western blots.

Protein oxidation

Protein oxidation assays from whole heart lysates were carried out using the OxyBlot Protein Oxidation Detection Kit (Millipore S7150) following the manufacturer's instructions.

Mitochondrial Ca^{2+} measurement

Mitochondrial Ca^{2+} handling was assessed using mitochondria-localized, ratiometric-pericam (MitoPericam) or Mitycam, as previously described (8, 34, 55). AAV containing MitoPericam or Mitycam gene sequences were expressed for 4 weeks before the mitochondrial Ca^{2+} measurements were performed in isolated adult CM.

$[Ca^{2+}]_m$ in intact CM with MitoPericam

Data were collected from paced-contracting individual CM from the emission channel at a rate of 20 Hz and the ratio between the intensities of the two excitations (410/485) was calculated providing for relative comparisons of the $[Ca^{2+}]_m$ between experimental treatments. $[Ca^{2+}]_m$ was determined as described (56). Calibration of the MitoPericam signal to molar $[Ca^{2+}]_m$ was done as described (56). Basal $[Ca^{2+}]_m$ was obtained from paced myocytes averaging diastolic and systolic $[Ca^{2+}]_m$, which are the minimum and maximum pericam ratios, respectively, that were measured during contraction.

Mitochondrial Ca^{2+} transients in intact CM with Mitycam

Fluorescence was measured with excitation at 488 nm (emission between 545 $\pm$ 50 nm) using the system described for MitoPericam. Mitycam measurement was performed as described by Lu *et al.* (57). Analysis of mitochondrial Ca^{2+} transients was performed as described (34, 58). Ca^{2+} uptake is the maximum slope of the upstroke. Ca^{2+} release is the maximum slope during Ca^{2+} decline.

Ca^{2+} content in permeabilized CM

Ca^{2+} content in permeabilized CM was performed as described (59). Isolated adult CM were transferred to a Ca^{2+}-free medium containing thapsigargin (sarcoplasmic reticulum Ca^{2+}-APTase inhibitor), digitonin, protease inhibitors, and succinate, pH 7.2. Digitonin-permeabilized CM were treated with Ru360 (MCU inhibitor) and CGP-37157 (mNCLX inhibitor) to inhibit mitochondrial Ca^{2+} exchange. FCCP was added to disrupt the $\Delta\psi_m$ and release all free mitochondrial matrix Ca^{2+} and detected by Fura-2.

$\Delta\psi_m$ in isolated CM

$\Delta\psi_m$ was measured deploying the cationic carbocyanine JC-1 dye, as described previously (60).

PDC activity

Pyruvate dehydrogenase complex activity was assessed from whole heart homogenates using the PDC Enzyme Activity Microplate Assay Kit from Abcam (ab109902) following the manufacturer's instructions.

Mitochondrial O_2 respiration

Mitochondrial respiration was measured with a Clark-type electrode (YSI) as described (61). Basal respiration was measured with succinate (10 mM) as substrate, 2 μM rotenone was present in the basal condition (state 4). 4 mM ADP was added to produce state 3 respiration, as previously described (62). RCR was calculated as ratio of state 3:state 4 respiration.

NMR analysis of mitochondrial ATP production

ATP production was monitored using the 2DG ATP energy clamp method as described (37).

Energy substrate metabolism in the Neely working heart model

Glucose and fatty acid metabolism were measured in isolated working hearts as described previously (8). Briefly, hearts were perfused with a modified Krebs-Henseleit buffer containing 11 mM glucose and 0.8 mM palmitate bound to 3% BSA (fatty acid free). [5-^{3}H]Glucose was used to measure glucose oxidation and [9,10-^{3}H]palmitate to measure fatty acid oxidation.

Metabolomics analysis

LC–MS/MS analysis was used to measure metabolites. Blood was harvested from heparinized mice before heart excision and plasma was extracted using standard protocols. Excised hearts were rinsed in ice-cold PBS and snap frozen. Frozen heart samples were transferred to a 2.0-ml impact-resistant tube containing 200 mg of 1-mm zirconium beads. To each tube, 50 μl/mg of ice-cold 80:20 methanol:water was added. This was followed by two 3 $\times$ 15-s homogenization cycles at 6,400 Hz in a Precellys 24® tissue homogenizer. For the plasma, 40 μl was added to 160 μl of ice-cold 80:20 methanol:water to extract metabolites and precipitate protein. The heart and plasma samples were then placed in the −20 °C freezer for 30 min to allow for precipitation of protein. Samples were thereafter vortexed for 30 s, centrifuged at 14,000 $\times$ *g* for 10 min at 4 °C, and supernatants were transferred to LC–MS vials containing a 200-μl glass inserts. All samples were kept at 4 °C in the autosampler compartment until 2 μl was injected for analysis. LC–MS-based metabolomics analysis was performed using a Thermo QExactive orbitrap mass spectrometer coupled to a Thermo Vanquish UPLC system. Chromatographic separation of metabolites was achieved using a Millipore (Sequant) Zic-pHILIC 2.1 $\times$ 150-mm, 5-μm column maintained at 25 °C using a flow rate of 0.3 ml/min. Compounds were eluted via a 19-min linear gradient

starting from 90:10 acetonitrile: 20 mM ammonium bicarbonate to 45:55 acetonitrile: 20 mM ammonium bicarbonate. A Thermo Q-Exactive orbitrap mass spectrometer was operated in positive and negative ion modes using a heated electrospray ionization (HESI) source at 35,000 resolution, 100-ms ion trap time for MS1 and 17,500 resolution, 50-ms ion trap time for MS2 collection. Data were collected over a mass range of m/z 67–1000, using a sheath gas flow rate of 40 units, auxillary gas flow rate of 20 units, sweep gas flow rate of 2 units, spray voltage of 3.5 and 2.5 kV for positive and negative ion modes, respectively, capillary inlet temperature of 275 °C, auxillary gas heater temperature of 350 °C, and an S-lens RF level of 45. For the MS2 collection, MS1 ions were isolated using a 1.0 m/z window and fragmented using a normalized collision energy of 35. Fragmented ions were placed on dynamic exclusion for 30 s before being allowed to be fragmented again. Collected data were imported into the mzMine 2.20 software suite for analysis. A Log2-fold change adjustment followed by a z-score adjustment was done. The metabolites plotted were filtered by doing a t test between the control and diabetic groups and the metabolites that had a p value below 0.05 were further analyzed. From this heat maps for plasma and heart were generated using Morpheus by the Broad Institute (https://software.broadinstitute.org/morpheus/).[4] Hierarchical clustering between samples was done by a −1 Spearman rank correlation. Distance between clusters was measured by average. Glucose was identified using comparison of accurate mass, retention time, and MS2 features with pure standards, with relative quantitation of levels using MS1 intensity values.

Statistical analysis

Results are presented as mean ± S.D. One-way ANOVA with appropriate post hoc test, or unpaired Student's t test for comparison between two groups, were used. Gaussian distribution was always assumed. $p < 0.05$ was considered to be statistically significant.

Author contributions—J. S., F. C., B. T. S., J. D.-J., T. D., A. D., J. A. S., M. J., and W. H. D. conceptualization; J. S., F. C., B. T. S, K. L., J. D.-J., T. D., J. A. S., and M. J. data curation; J. S., F. C., B. T. S., K. L., J. D.-J., T. D., A. D., J. A. S., M. J., and W. H. D. formal analysis; J. S., F. C., B. T. S., T. D., J. A. S., M. J., and W. H. D. supervision; J. S., F. C., B. T. S., T. D., J. A. S., M. J., and W. H. D. validation; J. S., F. C., B. T. S., K. L., J. D.-J., T. D., A. D., J. A. S., M. J., and W. H. D. investigation; J. S., F. C., B. T. S., K. L., J. D.-J., T. D., A. D., J. A. S., M. J., and W. H. D. visualization; J. S., F. C., B. T. S., T. D., J. A. S., M. J., and W. H. D. methodology; J. S., F. C., and B. T. S. writing-original draft; J. S., F. C., B. T. S., M. J., and W. H. D. project administration; J. S., F. C., B. T. S., K. L., J. D.-J., T. D., J. A. S., M. J., and W. H. D. writing-review and editing; F. C., J. D.-J., A. D., M. J., and W. H. D. funding acquisition.

Acknowledgments—We thank Dr. Godfrey Smith (University of Glasgow, Glasgow, United Kingdom) and Dr. Shey-Shing Sheu (Thomas Jefferson University, Philadelphia, PA) for the kind gifts of the Mito-Pericam and Mitycam genes used in these studies.

[4] Please note that the JBC is not responsible for the long-term archiving and maintenance of this site or any other third party hosted site.

References

1. Schilling, J. D. (2015) The mitochondria in diabetic heart failure: from pathogenesis to therapeutic promise. *Antioxid. Redox Signal.* **22,** 1515–1526 Medline
2. Tanaka, Y., Konno, N., and Kako, K. J. (1992) Mitochondrial dysfunction observed *in situ* in cardiomyocytes of rats in experimental diabetes. *Cardiovasc. Res.* **26,** 409–414 CrossRef Medline
3. Flarsheim, C. E., Grupp, I. L., and Matlib, M. A. (1996) Mitochondrial dysfunction accompanies diastolic dysfunction in diabetic rat heart. *Am. J. Physiol. Heart Circ. Physiol.* **271,** H192–H202 CrossRef
4. Sloan, R. C., Moukdar, F., Frasier, C. R., Patel, H. D., Bostian, P. A., Lust, R. M., and Brown, D. A. (2012) Mitochondrial permeability transition in the diabetic heart: contributions of thiol redox state and mitochondrial calcium to augmented reperfusion injury. *J. Mol. Cell. Cardiol.* **52,** 1009–1018 CrossRef Medline
5. Glancy, B., and Balaban, R. S. (2012) Role of mitochondrial Ca^{2+} in the regulation of cellular energetics. *Biochemistry* **51,** 2959–2973 CrossRef Medline
6. Denton, R. M. (2009) Regulation of mitochondrial dehydrogenases by calcium ions. *Biochim. Biophys. Acta* **1787,** 1309–1316 CrossRef Medline
7. Rutter, G. A., Midgley, P. J., and Denton, R. M. (1989) Regulation of the pyruvate dehydrogenase complex by Ca^{2+} within toluene-permeabilized heart mitochondria. *Biochim. Biophys. Acta* **1014,** 263–270 CrossRef Medline
8. Belke, D. D., Swanson, E., Suarez, J., Scott, B. T., Stenbit, A. E., and Dillmann, W. H. (2007) Increased expression of SERCA in the hearts of transgenic mice results in increased oxidation of glucose. *Am. J. Physiol. Heart Circ. Physiol.* **292,** H1755–H1763 CrossRef Medline
9. Neely, J. R., Rovetto, M. J., and Oram, J. F. (1972) Myocardial utilization of carbohydrate and lipids. *Prog. Cardiovasc. Dis.* **15,** 289–329 CrossRef Medline
10. Griffin, T. M., Humphries, K. M., Kinter, M., Lim, H. Y., and Szweda, L. I. (2016) Nutrient sensing and utilization: Getting to the heart of metabolic flexibility. *Biochimie* **124,** 74–83 CrossRef
11. Bugger, H., and Abel, E. D. (2009) Rodent models of diabetic cardiomyopathy. *Dis. Model Mech.* **2,** 454–466 CrossRef Medline
12. Weiss, J. N., and Lamp, S. T. (1989) Cardiac ATP-sensitive K^+ channels: evidence for preferential regulation by glycolysis. *J. Gen. Physiol.* **94,** 911–935 CrossRef Medline
13. Entman, M. L., Bornet, E. P., Van Winkle, W. B., Goldstein, M. A., and Schwartz, A. (1977) Association of glycogenolysis with cardiac sarcoplasmic recticulum: II. effect of glycogen depletion, deoxycholate solubilization and cardiac ischemia: evidence for a phosphorylase kinase membrane complex. *J. Mol. Cell. Cardiol.* **9,** 515–528 CrossRef Medline
14. Weiss, J. N., and Lamp, S. T. (1987) Glycolysis preferentially inhibits ATP-sensitive K^+ channels in isolated guinea pig cardiac myocytes. *Science* **238,** 67–69 CrossRef Medline
15. Randle, P. J., Garland, P. B., Hales, C. N., and Newsholme, E. A. (1963) The glucose fatty-acid cycle: its role in insulin sensitivity and the metabolic disturbances of diabetes mellitus. *Lancet* **1,** 785–789 Medline
16. Mor, I., Cheung, E. C., and Vousden, K. H. (2011) Control of glycolysis through regulation of PFK1: old friends and recent additions. *Cold Spring Harb. Symp. Quant. Biol.* **76,** 211–216 CrossRef Medline
17. Andrienko, T. N., Picht, E., and Bers, D. M. (2009) Mitochondrial free calcium regulation during sarcoplasmic reticulum calcium release in rat cardiac myocytes. *J Mol. Cell Cardiol.* **46,** 1027–1036 CrossRef Medline
18. Gunter, T. E., and Pfeiffer, D. R. (1990) Mechanisms by which mitochondria transport calcium. *Am. J. Physiol.* **258,** C755–C786 CrossRef Medline
19. Rizzuto, R., Pinton, P., Carrington, W., Fay, F. S., Fogarty, K. E., Lifshitz, L. M., Tuft, R. A., and Pozzan, T. (1998) Close contacts with the endoplasmic reticulum as determinants of mitochondrial Ca^{2+} responses. *Science* **280,** 1763–1766 CrossRef Medline
20. Santo-Domingo, J., and Demaurex, N. (2010) Calcium uptake mechanisms of mitochondria. *Biochim. Biophys. Acta* **1797,** 907–912 CrossRef Medline

21. De Stefani, D., Raffaello, A., Teardo, E., Szabò, I., and Rizzuto, R. (2011) A 40-kilodalton protein of the inner membrane is the mitochondrial calcium uniporter. *Nature* **476,** 336–340 CrossRef Medline
22. Baughman, J. M., Perocchi, F., Girgis, H. S., Plovanich, M., Belcher-Timme, C. A., Sancak, Y., Bao, X. R., Strittmatter, L., Goldberger, O., Bogorad, R. L., Koteliansky, V., and Mootha, V. K. (2011) Integrative genomics identifies MCU as an essential component of the mitochondrial calcium uniporter. *Nature* **476,** 341–345 CrossRef Medline
23. Perocchi, F., Gohil, V. M., Girgis, H. S., Bao, X. R., McCombs, J. E., Palmer, A. E., and Mootha, V. K. (2010) MICU1 encodes a mitochondrial EF hand protein required for Ca^{2+} uptake. *Nature* **467,** 291–296 CrossRef Medline
24. Plovanich, M., Bogorad, R. L., Sancak, Y., Kamer, K. J., Strittmatter, L., Li, A. A., Girgis, H. S., Kuchimanchi, S., De Groot, J., Speciner, L., Taneja, N., Oshea, J., Koteliansky, V., and Mootha, V. K. (2013) MICU2, a paralog of MICU1, resides within the mitochondrial uniporter complex to regulate calcium handling. *PLoS ONE* **8,** e55785 CrossRef Medline
25. Raffaello, A., De Stefani, D., Sabbadin, D., Teardo, E., Merli, G., Picard, A., Checchetto, V., Moro, S., Szabò, I., and Rizzuto, R. (2013) The mitochondrial calcium uniporter is a multimer that can include a dominant-negative pore-forming subunit. *EMBO J.* **32,** 2362–2376 CrossRef Medline
26. Sancak, Y., Markhard, A. L., Kitami, T., Kovács-Bogdán, E., Kamer, K. J., Udeshi, N. D., Carr, S. A., Chaudhuri, D., Clapham, D. E., Li, A. A., Calvo, S. E., Goldberger, O., and Mootha, V. K. (2013) EMRE is an essential component of the mitochondrial calcium uniporter complex. *Science* **342,** 1379–1382 CrossRef Medline
27. Liu, J. C., Liu, J., Holmström, K. M., Menazza, S., Parks, R. J., Fergusson, M. M., Yu, Z.-X., Springer, D. A., Halsey, C., Liu, C., Murphy, E., and Finkel, T. (2016) MICU1 serves as a molecular gatekeeper to prevent *in vivo* mitochondrial calcium overload. *Cell Rep.* **16,** 1561–1573 CrossRef Medline
28. Tomar, D., Dong, Z., Shanmughapriya, S., Koch, D. A., Thomas, T., Hoffman, N. E., Timbalia, S. A., Goldman, S. J., Breves, S. L., Corbally, D. P., Nemani, N., Fairweather, J. P., Cutri, A. R., Zhang, X., Song, J., *et al.* (2016) MCUR1 is a scaffold factor for the MCU complex function and promotes mitochondrial bioenergetics. *Cell Rep.* **15,** 1673–1685 CrossRef Medline
29. Beutner, G., Sharma, V. K., Giovannucci, D. R., Yule, D. I., and Sheu, S. S. (2001) Identification of a ryanodine receptor in rat heart mitochondria. *J. Biol. Chem.* **276,** 21482–21488 CrossRef Medline
30. Jiang, D., Zhao, L., and Clapham, D. E. (2009) Genome-wide RNAi screen identifies Letm1 as a mitochondrial Ca^{2+}/H^{+} antiporter. *Science* **326,** 144–147 CrossRef Medline
31. Palty, R., Silverman, W. F., Hershfinkel, M., Caporale, T., Sensi, S. L., Parnis, J., Nolte, C., Fishman, D., Shoshan-Barmatz, V., Herrmann, S., Khananshvili, D., and Sekler, I. (2010) NCLX is an essential component of mitochondrial Na^{+}/Ca^{2+} exchange. *Proc. Natl. Acad. Sci. U.S.A.* **107,** 436–441 CrossRef Medline
32. Bernardi, P., and von Stockum, S. (2012) The permeability transition pore as a Ca^{2+} release channel: new answers to an old question. *Cell Calcium* **52,** 22–27 CrossRef Medline
33. Williams, G. S., Boyman, L., Chikando, A. C., Khairallah, R. J., and Lederer, W. J. (2013) Mitochondrial calcium uptake. *Proc. Natl. Acad. Sci. U.S.A.* **110,** 10479–10486 CrossRef Medline
34. Diaz-Juarez, J., Suarez, J., Cividini, F., Scott, B. T., Diemer, T., Dai, A., and Dillmann, W. H. (2016) Expression of the mitochondrial calcium uniporter in cardiac myocytes improves impaired mitochondrial calcium handling and metabolism in simulated hyperglycemia. *Am. J. Physiol. Cell Physiol.* **311,** C1005–C1013 CrossRef
35. Pulicherla, N., Shen, S., Yadav, S., Debbink, K., Govindasamy, L., Agbandje-McKenna, M., and Asokan, A. (2011) Engineering liver-detargeted AAV9 vectors for cardiac and musculoskeletal gene transfer. *Mol. Ther.* **19,** 1070–1078 CrossRef Medline
36. Zincarelli, C., Soltys, S., Rengo, G., and Rabinowitz, J. E. (2008) Analysis of AAV serotypes 1–9 mediated gene expression and tropism in mice after systemic injection. *Mol. Ther.* **16,** 1073–1080 CrossRef Medline
37. Yu, L., Fink, B. D., Herlein, J. A., and Sivitz, W. I. (2013) Mitochondrial function in diabetes: novel methodology and new insight. *Diabetes* **62,** 1833–1842 CrossRef Medline
38. Ji, L., Liu, F., Jing, Z., Huang, Q., Zhao, Y., Cao, H., Li, J., Yin, C., Xing, J., and Li, F. (2017) MICU1 alleviates diabetic cardiomyopathy through mitochondrial Ca^{2+}-dependent antioxidant response. *Diabetes* **66,** 1586–1600 CrossRef Medline
39. Wang, B., Chandrasekera, P. C., and Pippin, J. J. (2014) Leptin- and leptin receptor-deficient rodent models: relevance for human type 2 diabetes. *Curr. Diabetes. Rev.* **10,** 131–145 CrossRef Medline
40. Allison, M. B., and Myers, M. G., Jr. (2014) 20 years of leptin: connecting leptin signaling to biological function. *J. Endocrinol.* **223,** T25–T35 CrossRef Medline
41. Ong, S.-B., Samangouei, P., Kalkhoran, S. B., and Hausenloy, D. J. (2015) The mitochondrial permeability transition pore and its role in myocardial ischemia reperfusion injury. *J. Mol. Cell. Cardiol.* **78,** 23–34 CrossRef Medline
42. Lopaschuk, G. D., Ussher, J. R., Folmes, C. D., Jaswal, J. S., and Stanley, W. C. (2010) Myocardial fatty acid metabolism in health and disease. *Physiol. Rev.* **90,** 207–258 CrossRef Medline
43. Pendin, D., Greotti, E., and Pozzan, T. (2014) The elusive importance of being a mitochondrial Ca^{2+} uniporter. *Cell Calcium* **55,** 139–145 CrossRef Medline
44. Granatiero, V., De Stefani, D., and Rizzuto, R. (2017) Mitochondrial Calcium Handling in Physiology and Disease. in *Mitochondrial Dynamics in Cardiovascular Medicine* (Santulli, G. ed) pp. 25–47, Springer International Publishing, Cham, Switzerland
45. Cividini, F., Scott, B. T., Dai, A., Han, W., Suarez, J., Diaz-Juarez, J., Diemer, T., Casteel, D. E., and Dillmann, W. H. (2016) *O*-GlcNAcylation of 8-oxoguanine DNA glycosylase (Ogg1) impairs oxidative mitochondrial DNA lesion repair in diabetic hearts. *J. Biol. Chem.* **291,** 26515–26528 CrossRef
46. Trost, S. U., Swanson, E., Gloss, B., Wang-Iverson, D. B., Zhang, H., Volodarsky, T., Grover, G. J., Baxter, J. D., Chiellini, G., Scanlan, T. S., and Dillmann, W. H. (2000) The thyroid hormone receptor-β-selective agonist GC-1 differentially affects plasma lipids and cardiac activity. *Endocrinology* **141,** 3057–3064 CrossRef Medline
47. Fang, H., Lai, N. C., Gao, M. H., Miyanohara, A., Roth, D. M., Tang, T., and Hammond, H. K. (2012) Comparison of adeno-associated virus serotypes and delivery methods for cardiac gene transfer. *Hum. Gene Ther. Methods* **23,** 234–241 CrossRef Medline
48. Wahlquist, C., Jeong, D., Rojas-Muñoz, A., Kho, C., Lee, A., Mitsuyama, S., van Mil, A., Park, W. J., Sluijter, J. P., Doevendans, P. A., Hajjar, R. J., and Mercola, M. (2014) Inhibition of miR-25 improves cardiac contractility in the failing heart. *Nature* **508,** 531–535 CrossRef Medline
49. Hu, Y., Belke, D., Suarez, J., Swanson, E., Clark, R., Hoshijima, M., and Dillmann, W. H. (2005) Adenovirus-mediated overexpression of *O*-GlcNAcase improves contractile function in the diabetic heart. *Circ. Res.* **96,** 1006–1013 CrossRef Medline
50. Belke, D. D., Swanson, E. A., and Dillmann, W. H. (2004) Decreased sarcoplasmic reticulum activity and contractility in diabetic db/db mouse heart. *Diabetes* **53,** 3201–3208 CrossRef Medline
51. Trost, S. U., Belke, D. D., Bluhm, W. F., Meyer, M., Swanson, E., and Dillmann, W. H. (2002) Overexpression of the sarcoplasmic reticulum Ca^{2+}-ATPase improves myocardial contractility in diabetic cardiomyopathy. *Diabetes* **51,** 1166–1171 CrossRef Medline
52. Das, A., Salloum, F. N., Filippone, S. M., Durrant, D. E., Rokosh, G., Bolli, R., and Kukreja, R. C. (2015) Inhibition of mammalian target of rapamycin protects against reperfusion injury in diabetic heart through STAT3 signaling. *Basic Res. Cardiol.* **110,** 31 CrossRef Medline
53. Fricovsky, E. S., Suarez, J., Ihm, S.-H., Scott, B. T., Suarez-Ramirez, J. A., Banerjee, I., Torres-Gonzalez, M., Wang, H., Ellrott, I., Maya-Ramos, L., Villarreal, F., and Dillmann, W. H. (2012) Excess protein *O*-GlcNAcylation and the progression of diabetic cardiomyopathy. *Am. J. Physiol. Regul. Integ. Comp. Physiol.* **303,** R689–R699 CrossRef
54. Suarez, J., Belke, D. D., Gloss, B., Dieterle, T., McDonough, P. M., Kim, Y.-K., Brunton, L. L., and Dillmann, W. H. (2004) *In vivo* adenoviral transfer of sorcin reverses cardiac contractile abnormalities of diabetic cardiomyopathy. *Am. J. Physiol. Heart Circ. Physiol.* **286,** H68–H75 CrossRef
55. Suarez, J., McDonough, P. M., Scott, B. T., Suarez-Ramirez, A., Wang, H., Fricovsky, E. S., and Dillmann, W. H. (2013) Sorcin modulates mitochon-

drial Ca^{2+} handling and reduces apoptosis in neonatal rat cardiac myocytes. *Am. J. Physiol. Cell Physiol.* **304,** C248–C256 CrossRef

56. Griesbeck, O., Baird, G. S., Campbell, R. E., Zacharias, D. A., and Tsien, R. Y. (2001) Reducing the environmental sensitivity of yellow fluorescent protein. *J. Biol. Chem.* **276,** 29188–29194 CrossRef
57. Lu, X., Ginsburg, K. S., Kettlewell, S., Bossuyt, J., Smith, G. L., and Bers, D. M. (2013) Measuring local gradients of intramitochondrial [Ca^{2+}] in cardiac myocytes during sarcoplasmic reticulum Ca^{2+} release. *Circ. Res.* **112,** 424–431 CrossRef Medline
58. Suarez, J., McDonough, P. M., Scott, B. T., Suarez-Ramirez, A., Wang, H., Fricovsky, E. S., and Dillmann, W. H. (2013) Sorcin modulates mitochondrial Ca^{2+} handling and reduces apoptosis in neonatal rat cardiac myocytes. *Am. J. Physiol. Cell Physiol.* **304,** C248–C256 CrossRef Medline
59. Luongo, T. S., Lambert, J. P., Yuan, A., Zhang, X., Gross, P., Song, J., Shanmughapriya, S., Gao, E., Jain, M., Houser, S. R., Koch, W. J., Cheung, J. Y., Madesh, M., and Elrod, J. W. (2015) The mitochondrial calcium uniporter matches energetic supply with cardiac workload during stress and modulates permeability transition. *Cell Rep.* **12,** 23–34 CrossRef Medline
60. 60 Makino, A., Suarez, J., Gawlowski, T., Han, W., Wang, H., Scott, B. T., and Dillmann, W. H. (2011) Regulation of mitochondrial morphology and function by *O*-GlcNAcylation in neonatal cardiac myocytes. *Am. J. Physiol. Regul., Integ. Comp. Physiol.* **300,** R1296–R1302 CrossRef
61. 61 Hu, Y., Suarez, J., Fricovsky, E., Wang, H., Scott, B. T., Trauger, S. A., Han, W., Oyeleye, M. O., and Dillmann, W. H. (2009) Increased enzymatic *O*-GlcNAcylation of mitochondrial proteins impairs mitochondrial function in cardiac myocytes exposed to high glucose. *J. Biol. Chem.* **284,** 547–555 CrossRef Medline
62. 62 Gottlieb, E., Armour, S. M., and Thompson, C. B. (2002) Mitochondrial respiratory control is lost during growth factor deprivation. *Proc. Natl. Acad. Sci. U.S.A.* **99,** 12801–12806 CrossRef Medline